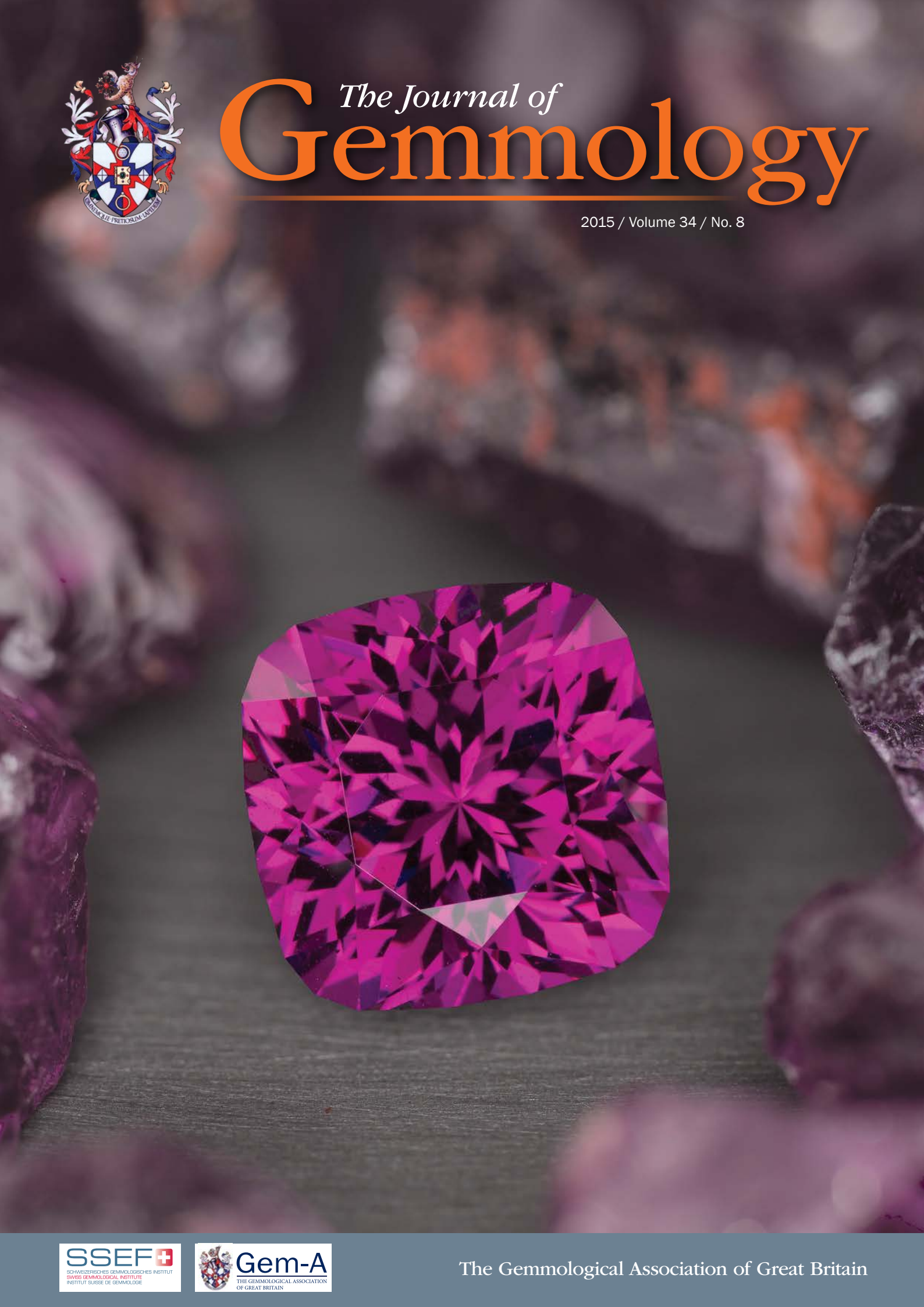

The Journal of Gemmology

2015 / Volume 34 / No. 8

SSEF
SCHWEIZERISCHES GEMMOLOGISCHES INSTITUT
SWISS GEMMOLOGICAL INSTITUTE
INSTITUT SUISSE DE GEMMOLOGIE

Gem-A
THE GEMMOLOGICAL ASSOCIATION OF GREAT BRITAIN

The Gemmological Association of Great Britain

From Exsolution to 'Gold Sheen': A New Variety of Corundum

Thanh Nhan Bui, Katerina Deliousi, Tanzim Khan Malik and Katrien De Corte

Sapphires displaying an attractive golden sheen reportedly were discovered in eastern Kenya in late 2009, and were recently brought to market in commercial quantities. The basic gemmological properties of the so-called Gold Sheen sapphires are consistent with typical corundum. Microscopic examination and Raman micro-spectroscopy showed that Fe-Ti oxides (hematite, ilmenite and magnetite) are the main solid inclusions, and they are oriented parallel to crystallographic directions in the basal pinacoid of corundum characterized by a six-fold rotational symmetry. Hematite and ilmenite are present in the form of exsolution intergrowths within platelets or needles. Magnetite typically appears as larger and thicker black platelets. The sheen effect in these sapphires originates from the simultaneous reflection of light from the oriented network of exsolved hematite-ilmenite inclusions.

The Journal of Gemmology, 34(8), 2015, pp. 678–691, http://dx.doi.org/10.15506/JoG.2015.34.8.678

Introduction

At the end of 2009, African gem brokers brought a new type of sapphire to the Bangkok gem market. While the rough material appeared dark and opaque overall, it displayed a peculiar weak golden shimmering effect on basal pinacoid surfaces. Author TKM, a gem cutter and dealer for over 25 years, identified a potential business opportunity in this sapphire, and entered into an exclusive selling agreement with the mine owner. The material reportedly was produced from pits measuring a few metres deep in eastern Kenya near the border with Somalia. From 2010 to 2014, the rough material was exported to Thailand. The deposit was subsequently exhausted, with only non-commercial-quality gems extracted during the past two years. About 25 tonnes of rough have been stockpiled in Bangkok, where experiments on cutting and polishing are being conducted to best emphasize the distinctive golden shimmer of this corundum. Its appearance led author TKM to name the stone 'Gold Sheen' sapphire; the gems also have been presented as 'Zawadi' sapphire by some suppliers (e.g. Laurs, 2015).

In this article, we present a detailed gemmological study of the Gold Sheen sapphires and their inclusions, and compare their properties to those of other sheen-displaying gems to further understand their distinctive optical effect.

Samples and Methods

For this study, author TKM supplied 105 samples of Gold Sheen sapphire with a total weight of 675 carats. The stones ranged from 1 to 30 ct.

Figure 1: These Gold Sheen sapphires, faceted into checkerboard cuts or polished as cabochons, weigh up to 30 ct each. The golden sheen, colour zoning and fracture patterns are present in various combinations. Photo by T. K. Malik.

Except for one rough sample, they were cut and polished as cabochons and faceted gemstones of various qualities with regard to the golden sheen effect (e.g. Figure 1). Most of the cabochons were double-sided and displayed a light yellow to golden six-rayed star under a point light source (e.g. Figure 2). The faceted gems were cut into various common and fancy shapes. Due to a lack of transparency in the material, the proportions of the crown and pavilion were optimized for weight rather than for brilliance. Some of the crowns displayed a modified brilliant style, but the majority were fashioned into checkerboard cuts. The cutting and polishing of the rough material was the only processing imposed on the stones. Therefore, the Gold Sheen sapphires and their visual effect are completely natural.

Figure 2: A golden six-rayed star is shown by this 25.06 ct cabochon of Gold Sheen sapphire. Photo by T. K. Malik.

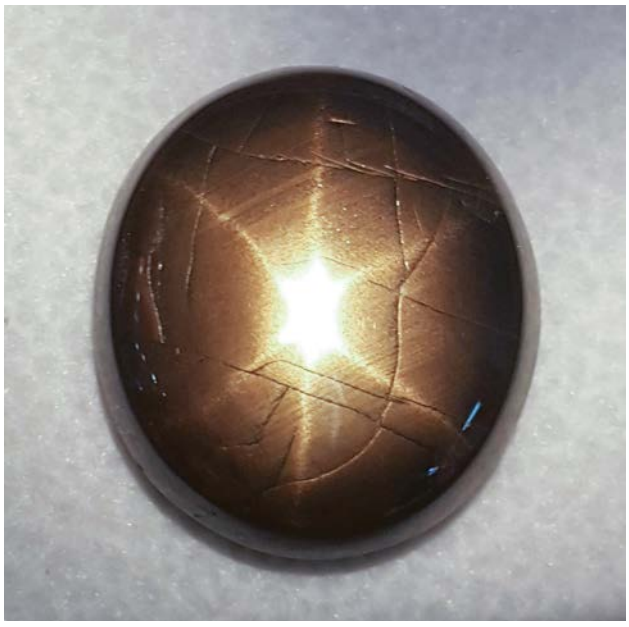

Basic gemmological characterization was performed on 46 samples at HRD Antwerp, and included visual observations, RI and hydrostatic SG measurements, polariscope and dichroscope reactions, hand-held spectroscope absorption spectra, and long- and short-wave UV fluorescence observations. In addition, the samples were studied with the D-Scope gemmological microscope from HRD Antwerp.

Energy-dispersive X-ray fluorescence (EDXRF) spectroscopy was achieved with a PANalytical Epsilon 5 instrument on 29 samples. For primary excitation, the Gd tube anode was operated with a current of 6–24 mA, a voltage of 25–100 kV and a power of 600 W, depending on the nine

secondary targets used for the emission of the different characteristic X-ray lines. The samples were analysed for 10–300 sec, focusing on the analytical X-ray line of each target according to the elements of interest. We used the *Kα* emission lines for most of the light trace elements and the *Lα* emission lines for elements with *Kα* lines greater than 20 keV.

Inclusions were identified in 20 samples using a Horiba LabRAM 800HR micro-Raman spectrometer at the Catholic University of Louvain (Louvain-la-Neuve, Belgium). Calibration was performed on a silicon substrate with a first-order Raman peak located at 520.7 cm^{-1}. A green laser (514 nm) was used to excite the samples, and its power was modulated to between 50% and 100%. The acquisition time for each spectrum ranged from 10 sec to 2 min, and each spectral acquisition was performed twice. Due to the very small size of the inclusions, we used magnifications of 500× and 1,000×. Raman spectra were normalized according to the most intense Raman peak, so as to plot several curves in the same graph. The background was not subtracted from the spectra.

The microstructure of the inclusions in one sample was investigated by a Zeiss Ultra55 field emission scanning electron microscope (SEM). We used a low accelerating voltage (2 keV) and the In-Lens secondary-electron detector with an optimized working distance (~2 mm) to obtain clear micrographs of the girdle profile of the sample where there was a high probability of surface-reaching needles and platelets. These parameters allowed us to resolve the cross-sections of the platelet inclusions to assess their thickness in SEM micrographs. The micrographs were horizontally aligned with the basal pinacoid and vertically aligned parallel to the c-axis of the corundum host.

All of the measurements were performed at ambient pressure and temperature, and none required any sample preparation.

Results

Visual Observations: Colour and Transparency

The body colour of the host sapphires was blue, green and/or yellow, with the latter being the most frequently encountered. The metallic sheen was characterized by a (golden) bronze colour that shimmered when the cabochons and faceted gems were illuminated. As demonstrated below, the shimmer was due to inclusions within the sapphires.

The c-axis of the corundum was oriented perpendicular to the crown/dome of the polished stones. Some samples displayed colour zoning in three orientations at 60°/120°, typical of the six-fold rotational symmetry in the basal plane of the rhombohedral system. Colour zoning in parallel lamellar patterns was created by layers containing various concentrations of inclusions that mechanically coloured those areas. Due to the reflection of light from the inclusions, those bands containing abundant particles appeared light, while the interstitial areas containing few inclusions showed the body colour of the sapphire, which generally appeared dark (especially for sapphires with blue body colour). Intermediate concentrations of inclusions exhibited a mixture of golden sheen and the body colour from the host sapphire.

Within areas showing the golden sheen, we typically observed dark surface-reaching cracks showing random paths. Their full extension was more visible when we observed the samples at an oblique angle to the surface of the stone.

In general, the diaphaneity of the sapphires varied according to the amount of sheen that they displayed. Samples showing less sheen were nearly transparent. Where the sheen was present over a larger area of a gemstone, the diaphaneity was translucent. In areas of darker bronze sheen, the stone could be completely opaque. This suggests that the inclusions responsible for the sheen also cause diminished transparency of the host sapphire.

Physical Properties

As the gemstones were heavily fractured, full of inclusions, typically translucent and not perfectly polished, routine gemmological testing was challenging. The overall results from the 46 samples were: RI—1.76–1.77 (spot reading), birefringence—0.01, SG—3.95–4.05, UV fluorescence—inert to long- and short-wave UV radiation, and spectroscope spectrum—absorption at 450 nm and in some samples a cutoff at ~500 nm. These are typical readings for corundum.

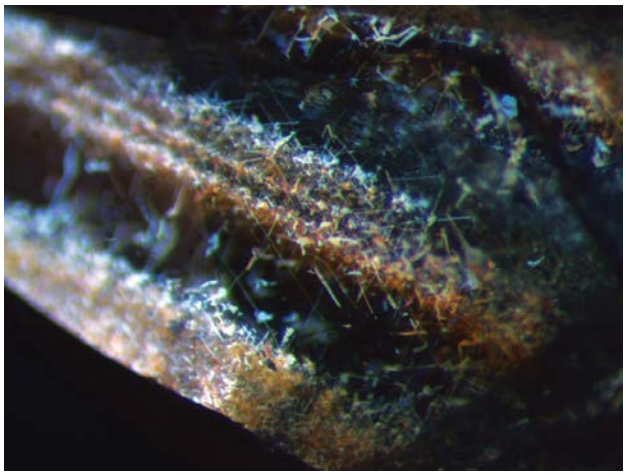

Figure 3: In areas of the sapphires showing sheen, networks of oriented inclusions consisting of needles and platelets lie within the basal pinacoid. Photomicrograph by T. N. Bui using brightfield illumination; magnified 60×, field of view 1.87 × 1.45 mm.

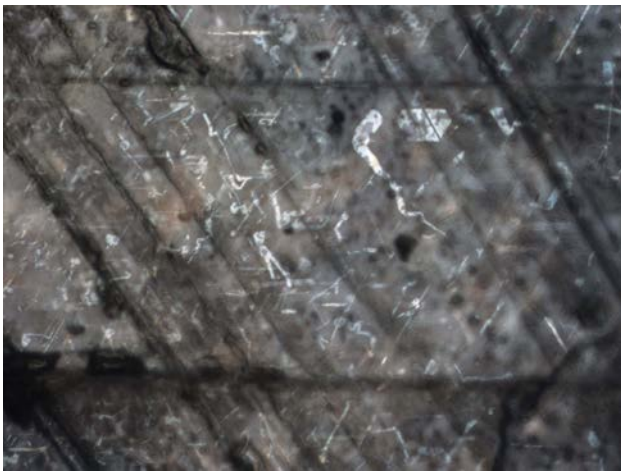

Figure 4: The surface of the basal pinacoid in this particular rough sapphire exhibits growth lines in three directions, parallel to {10$\bar{1}$0}. The needle inclusions below the surface are parallel to these growth lines. Photomicrograph by T. N. Bui using brightfield illumination; magnified 100×, field of view 860 × 635 µm.

Microscopic Characteristics

Under the gemmological range of magnification (10×–80×), we clearly observed hexagonal growth patterns and colour zoning in the sapphires. Furthermore, areas showing the sheen correlated to networks of numerous tiny straight needles and flakes lying within the corundum basal plane (Figure 3). In reflected light, the inclusions were golden metallic, and thus reflections from the inclusion networks created the golden sheen. In transmitted light, the inclusions appeared more orangy brown, and under oblique illumination they exhibited various colours due to thin-film interference (see Figure DD-1 in the Data Depository). The latter observation indicates an inclusion thickness in the nanometre range.

As mentioned above, the inclusions were present in three different orientations intersecting at 60°/120°, typical of the six-fold rotational symmetry in the basal plane of the rhombohedral system. These orientations also were parallel to the corundum growth lines (Figure 4), which are aligned along the first-order hexagonal prism {10$\bar{1}$0} (Hughes, 1997, p. 446). Also present in some samples were larger platelets that contained small dark areas (Figure 5).

Zones in the sapphires consisted of alternating bands of needles and platelets of different concentrations, at various positions along the c-axis (Figure 6). The bands containing inclusions of higher density and closer to the surface produced a golden bronze colour, while those of lower density and deeper inside the host produced a brownish bronze sheen, which resulted from a combination of reflections from the inclusions and the dark body colour of the host sapphire. This is well illustrated by comparing the appearance of a thin sample in reflected vs. transmitted light (again, see Figure 6).

Less abundant, but always present within the inclusion networks in the golden sheen areas, were black plates that were a similar size or larger than the platelets described above (Figure

Figure 5: The platelets in this sapphire contain dark areas and appear to be composed of different minerals. Photomicrograph by T. N. Bui using brightfield illumination; magnified 50×, field of view 1.3 × 1.0 mm.

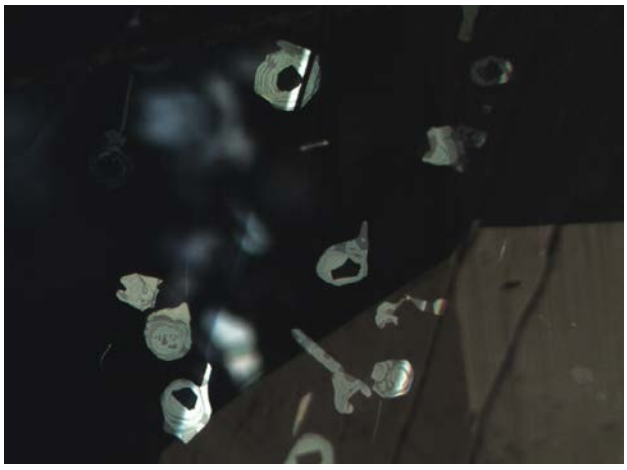

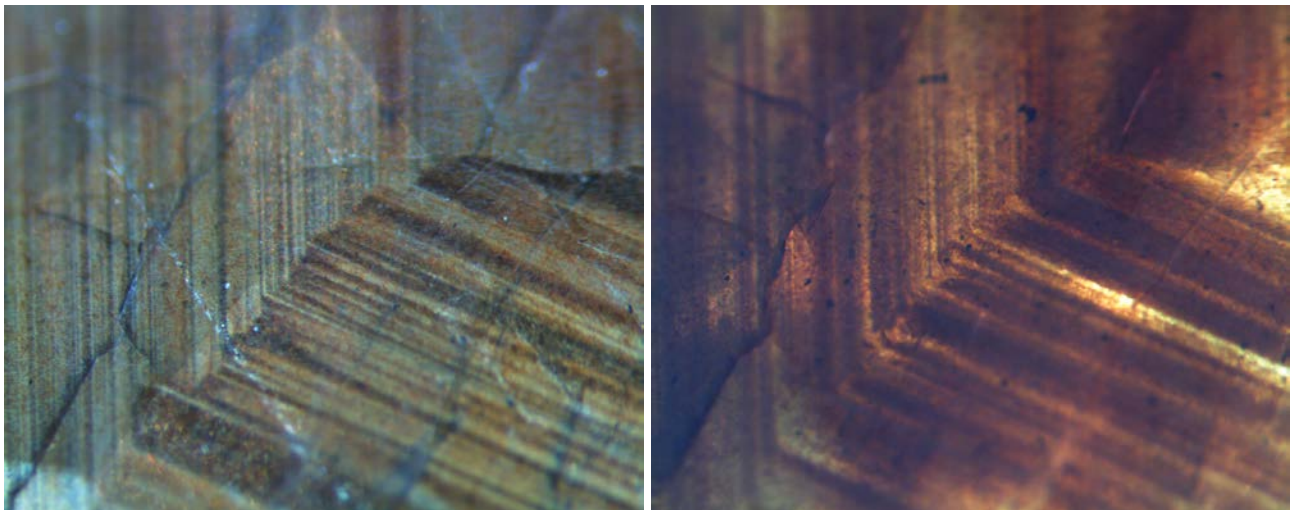

Figure 6: Colour zoning in this sapphire is characterized by different bronze colorations along the crystallographic directions of the corundum host (left, brightfield illumination). With transmitted light, the golden bronze-coloured bands appear dark and the brownish bronze-coloured bands are bright (right). This highlights variations in the concentration of needle and platelet inclusions along the c-axis. Photomicrographs by T. N. Bui; magnified 30×, field of view 4.76 × 3.81 mm.

7). Some of them were so large that they were visible to the naked eye, negatively affecting the appearance of the gemstone. The edges of these hexagonal-shaped inclusions were clearly parallel to the other inclusions and to the colour zoning.

The characteristics of the fractures within the sheen areas became more obvious when viewed with magnification. Their macroscopic 'dark vein' appearance correlated to the absence of inclusions around them. This indicates that these cracks were not created during the cutting of the stones. The absence of inclusions was evident only on one side of the fractures, characterized by a gradual increase in inclusion density away from the fractures. This asymmetry induced a colour gradient on one side leading up to the sharp boundary line of the fracture (Figure 8). This was easily observed with the naked eye in samples containing larger veins. Further microscopic investigations, combining brightfield and darkfield illuminations, showed a correlation between the asymmetry of the dark veins and the pattern of the associated fractures. The side of the dark vein presenting a concentration gradient of inclusions corresponded to the curvature direction

Figure 7: Black plates are present along with the network of needles and platelets in the Gold Sheen sapphires. These plates do not contribute to the sheen. Some of their borders are parallel to the orientation of the needles. Photomicrograph by K. Deliousi using transmitted light; magnified 80×, field of view 1.64 × 1.31 mm.

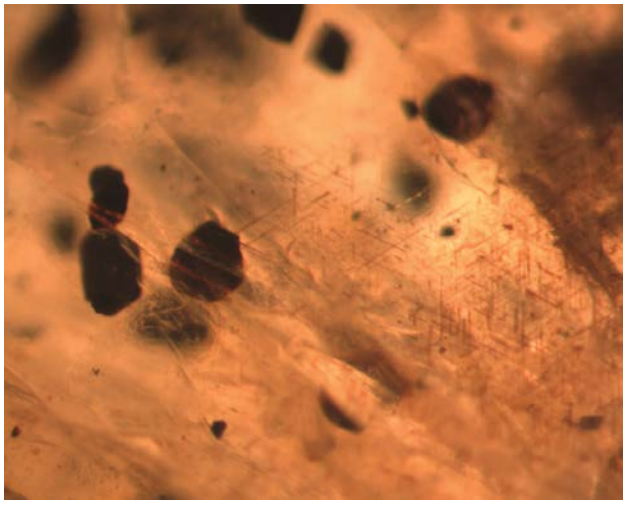

Figure 8: Surface-reaching fractures in the sheen area of the sapphires are characterized by asymmetric dark veins. Photomicrograph by K. Deliousi using brightfield illumination; magnified 25×, field of view 5.67 × 3.85 mm.

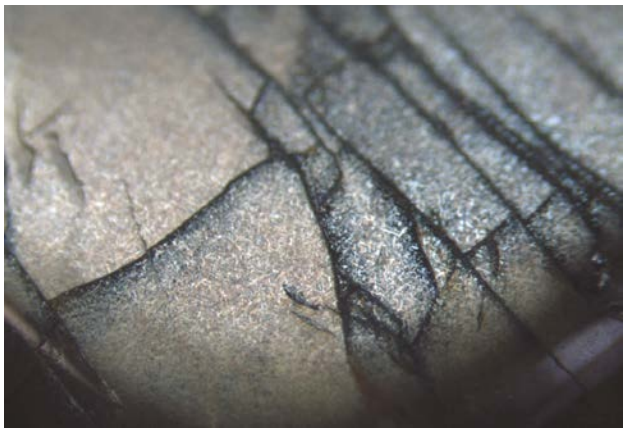

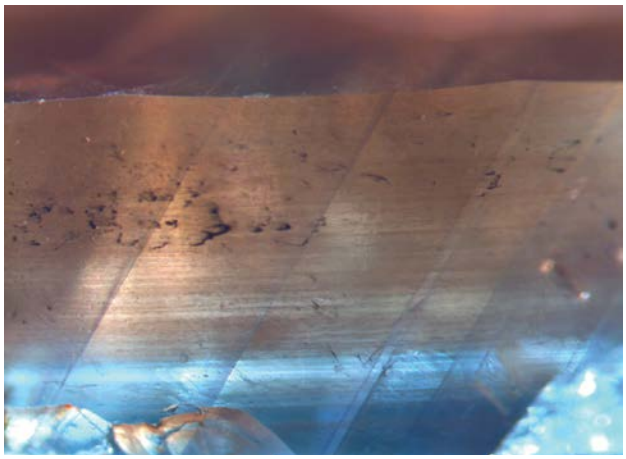

Figure 9: This view of the girdle of a Gold Sheen sapphire shows parallel brownish lines representing networks of needle and platelet inclusions along the basal pinacoid, and also a set of parallel lines (polysynthetic twin planes) oriented at about 58° and 32° to the basal pinacoid and the c-axis, respectively. Photomicrograph by T. N. Bui using darkfield illumination; magnified 30×, field of view 4.76 × 3.35 mm.

of the fracture. The distance along which the gradient extended was proportional to the slope of the fracture curvature. The asymmetric dark veins thus constituted an indirect mapping of the cracks underneath, shadowed by the inclusions.

Some samples showed a series of parallel lines when viewed at certain angles along the girdle profile (in a direction perpendicular to the c-axis). The angle between the lines and the basal pinacoid was 58° and that between the lines and the c-axis was 32° (Figure 9). These parallel lines are attributed to polysynthetic twin planes corresponding to the rhombohedral $\{10\bar{1}1\}$ faces of corundum. We observed parallel long white needles coincident with these twin planes when we looked through the table of the gemstones in a direction close to the c-axis (see Figure DD-2).

Due to the limited transparency of the gems, other solid inclusions were difficult to locate and identify. However, some surface-reaching inclusions in the lower-quality samples are described further below. In addition, planar assemblages of negative crystals corresponding to healed fractures were seen in some samples (e.g. Figures DD-3 and DD-4).

Chemical Composition

Qualitative EDXRF spectroscopy revealed the presence of the following trace elements in all 29 samples analysed: Fe, Ti, V, Cr, Ga, Nb and Ta. A relatively large amount of Fe suggested that this element was probably the main ingredient of the inclusions, especially in the networks of needles and platelets.

There was no obvious correlation between the blue body colour of some of the sapphires and the presence of Ti, as peaks of a similar intensity were also present in samples showing yellow and green body colours. Therefore, Ti could mainly be attributed to the inclusions. Other trace elements that are usually encountered as impurities in corundum include Ga, Nb and Ta; their concentrations varied in our samples.

Some of the sapphires, particularly those of low quality, contained additional trace elements including Zr, S, Ba, Cu, K, Na and Si. These may be attributed to various inclusions other than the metallic-appearing needles and platelets.

Inclusion Observations under High Magnification, and Raman Identification

Raman micro-spectroscopy is a powerful tool for identifying microscopic inclusions that are located at or near the surface of a gemstone (Bersani and Lottici, 2010; Kiefert and Karampelas, 2011). Since some inclusions had lateral dimensions of only a few microns, we used an optical magnification of 1,000× in order to obtain a laser spot of 1 µm. All of the analysed inclusions could be successfully identified by comparing their Raman spectra to those in the RRUFF database.

The high density of the inclusions responsible for the golden sheen makes them suitable for investigation through Raman spectroscopy. In most cases, the networks of needles and platelets reached the surface of the gems, or were less than 5 µm from the surface. Individual needles/platelets had such narrow thicknesses (less than 100 nm) that their surface-reaching cross-sections were extremely small to analyse, so it worked better to look for those that were located just under the surface. The particles selected for analysis had no intervening inclusions between them and the surface, nor ones situated directly below them. Therefore, the Raman spectra consisted exclusively of the superimposition of signals from both the sapphire and the inclusion. Figure 10a shows the spectrum of a host sapphire (α-Al_2O_3

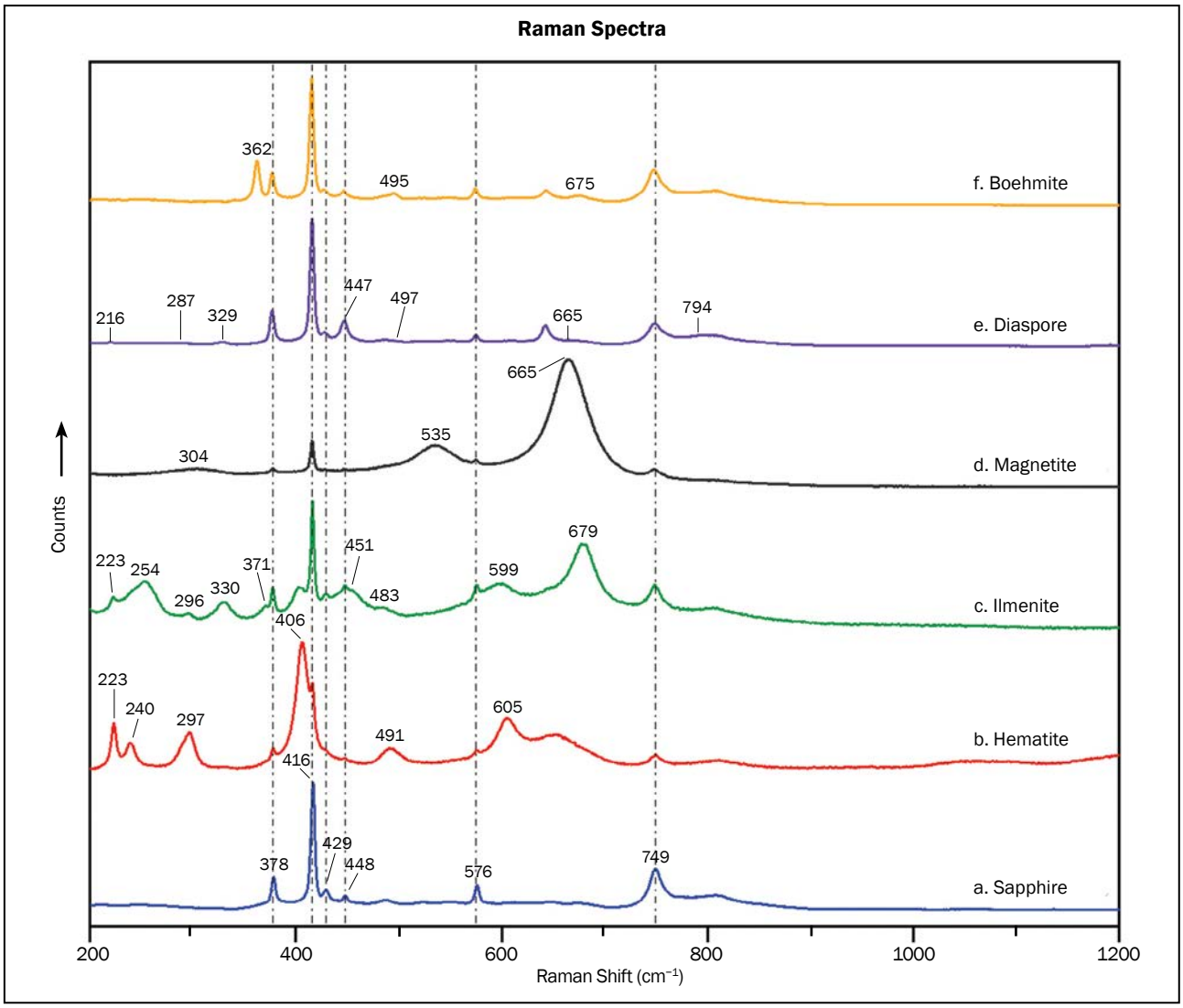

Figure 10: Raman spectra are shown for a host sapphire (a) and for various inclusions (b–f). The vertical dashed lines indicate the Raman peaks of corundum superimposed on those of the analysed inclusions. The two minerals present in the exsolved needles and platelets are hematite and ilmenite. Larger and thicker black plates were identified as magnetite. Diaspore and boehmite are the two polymorphs of AlO(OH) present in long white needles formed along the polysynthetic twin planes. (A peak that is present at 642 cm^{-1} in the spectra of both diaspore and boehmite is due to the A1g vibrational mode of the host corundum. These were the only spectra taken with the laser beam not perpendicular to the basal plane of the corundum.)

corundum), free of inclusions. In agreement with earlier studies (e.g. Xu et al., 1995), it includes peaks at 378, 416, 429, 448, 576 and 749 cm^{-1}.

The built-in optical microscope of the Raman micro-spectrometer, with magnifications from 200× to 1,000×, permitted us to identify some features that were barely distinguishable even when using the highest magnification of a typical gemmological microscope. Examples are provided by the needles and platelets illustrated in Figure 11. Several dark areas of various size and abundance were seen on many of the platelet inclusions. The duality of the colours within each inclusion suggested the presence of two different materials in the platelets. By contrast, in most cases the needles were of uniform colour, so they probably consisted of just one mineral. However, as the thickness of the needles increased, the probability was higher of observing colour inhomogeneities that may correspond to different minerals.

The platelets showed polygonal shapes with some of their edges parallel to the needles and other edges perpendicular to them. These edges were in turn parallel to the faces of the first- and second-order hexagonal prisms, {10$\bar{1}$0} and {11$\bar{2}$0},

Figure 11: The platelets and larger needles in the Gold Sheen sapphire consist of hematite and ilmenite (light and dark, respectively, in reflected light). The lighter areas (hematite) of the inclusions may display various colours due to thin-film interference from the nanometre-scale thickness of the inclusions. Two or more colours may be seen on the same platelet, indicating a variation in thickness (top right and bottom left). The darker areas (ilmenite) may also exhibit colour variations depending on thickness, but they are not as evident. Photomicrographs by T. N. Bui using brightfield illumination; magnified 1,000×, field of view 80 × 60 µm.

of the rhombohedral corundum host. The angles between two edges of the same polygon thus have the following possible values: 30°/150°, 60°/120° and 90°. Depending on the sample, the lateral dimensions of the platelets ranged from just a few to hundreds of micrometres. In SEM images, we observed a series of short white lines parallel to the basal pinacoid, corresponding to the needle-like and platelet inclusions. High magnification (100,000×) revealed the thickness of these inclusions was around 100 nm (Figure 12).

Raman micro-spectroscopy identified the smaller needles and the light-coloured areas of the platelets as hematite (α-Fe_2O_3), with the largest Raman peak at 406 cm^{-1} located near to that of sapphire, and other peaks recorded at 223, 240, 297, 491 and 605 cm^{-1} (Figure 10b). This is in good agreement with previous work on hematite (e.g. de Faria et al., 1997). Raman spectra of the dark areas of the platelets, characterized by a strong band at 679 cm^{-1}, were assigned to ilmenite ($FeTiO_3$); the other vibration modes describing this mineral were 223, 254, 296, 330, 371, 451, 483 and 599 cm^{-1} (Figure 10c). The obtained spectra are in good agreement with natural ilmenite for the main Raman peaks (e.g. Rull et al., 2004, 2007) and with pure synthesized ilmenite for the weaker Raman peaks (e.g. Sharma et al., 2009; Guan et al., 2013).

As mentioned previously, some black plates also were present in the golden sheen areas. The deep boundaries and terraces on the surfaces of these inclusions indicated that they are relatively thick (at the micron scale). Their

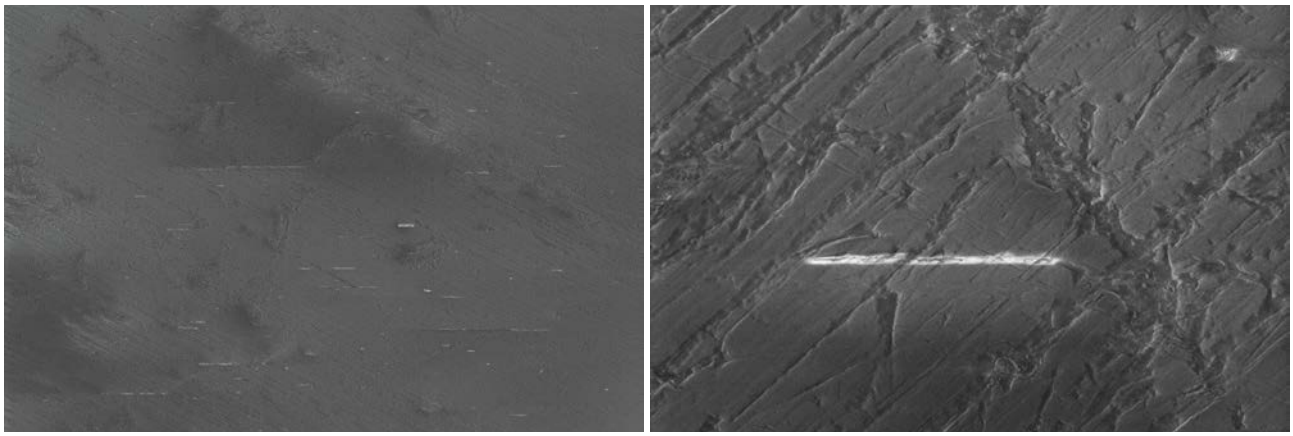

Figure 12: Cross-sections of platelet inclusions are observed in these SEM images taken from the girdle of a Gold Sheen sapphire. They appear as light grey thin parallel lines of various lengths at several levels along the c-axis (left). Closer examination of a single platelet inclusion (right) with the SEM shows that its thickness is 83 nm. Electron micrographs by T. N. Bui; magnified 2,000× (field of view 150 × 100 µm, left side), 20,000× (15 × 10 µm, right side).

lateral dimensions were generally greater than the hematite-ilmenite platelets. Observations with the Raman microscope confirmed their polygonal shape, with edges showing the same orientations as the platelets (Figure 13). Raman micro-spectroscopy identified these black inclusions as magnetite (Fe_3O_4), with three characteristic peaks at 304, 535 and 665 cm^{-1}, the latter being the strongest (Figure 10d). The obtained Raman spectra compared well to previous investigations on magnetite (de Faria et al., 1997).

The long needles lying along the polysynthetic twin planes were seen at high magnification to consist of tiny particles rather than a monocrystalline mineral. The concentration of these particles was higher toward the central core of the needle (Figure 14). Raman spectra obtained from different locations of several needles showed that the particles consisted of two polymorphs of aluminium oxide hydroxide. Most common was diaspore [α-AlO(OH)], with peaks at 216, 287, 329, 447 (strongest), 497, 665, 794 and 1191 cm^{-1} (Figure 10e). Occasionally, we found boehmite [γ-AlO(OH)], characterized by three Raman peaks at 362, 495 and 675 cm^{-1}, the first being the most intense (Figure 10f). All of these Raman features are in good agreement, for example, with a study on naturally occurring diaspore and synthesized boehmite (Ruan et al., 2001).

Several additional surface-reaching minerals were identified that did not contribute to the golden sheen: pyrite, baryte, covellite, zircon, muscovite, albite and K-feldspar. Photomicrographs and/or Raman spectra of these inclusions are provided in the Data Depository (Figures DD-5 to DD-7).

Discussion

Inclusions in the Gold Sheen Sapphires

The physical properties measured for the sapphires were not affected by the presence of their abundant inclusions. The concentration or weight of the inclusions was negligible in regard to the sapphire host, and the SG, RI and birefringence remained consistent with corundum. Optical microscopy highlighted the presence of a network of metallic-appearing needles and platelets and some larger black plates. Raman spectroscopy identified those inclusions as the Fe-Ti oxides hematite, ilmenite and magnetite. The presence of these inclusions in areas showing the golden sheen is consistent with the overall relatively high concentration of Fe (and Ti) in these sapphires.

The alignment of the colour zoning and the networks of hematite-ilmenite needles along the second- and first-order hexagonal prisms, $\{11\bar{2}0\}$ and $\{10\bar{1}0\}$ respectively, is consistent with previous studies of similar inclusions in black sapphires from Australia (Moon and Phillips, 1984). In that article, it was estimated from energy-dispersive spectroscopy that the exsolved inclusions consisted ~50% each of hematite and ilmenite. This is in reasonable agreement with high-magnification observations of the inclusions in our samples, although we noted a slightly higher amount of hematite (e.g. Figure 11).

Figure 13: Black plates in the Gold Sheen sapphires were identified as magnetite. The edges of the inclusions are aligned along the first- and second-order hexagonal prisms. Photomicrographs by T. N. Bui using brightfield illumination; magnified 500× or field of view 175 × 130 µm (top left, top right and bottom left) and 1,000× or 80 × 60 µm (bottom right).

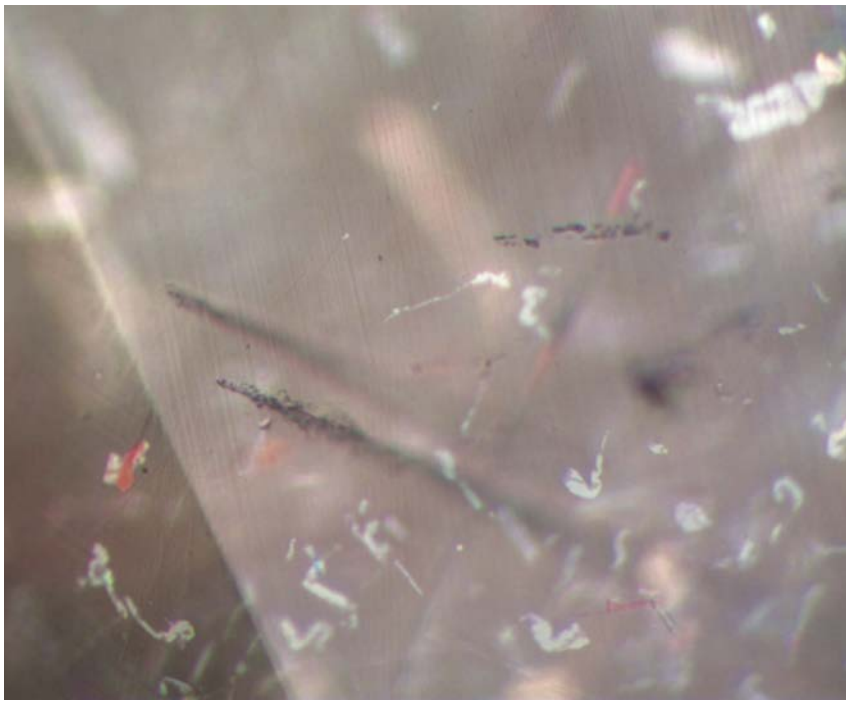

Figure 14: Needle-like inclusions consisting of diaspore and boehmite particles (appearing dark in brightfield illumination) lie along polysynthetic twin planes in the Gold Sheen sapphire. Photomicrograph by T. N. Bui; magnified 200×, field of view 360 × 300 µm.

As observed previously, in contrast to the needles, the edges of the platelets showing polygonal shapes were mostly parallel to both the first- and second-order hexagonal prisms of the host corundum. This difference highlights the preferential growth of the needles along the <10$\bar{1}$0> direction, probably due to the structural mismatch between the Fe-Ti oxides and corundum. The in-plane orientation of the hematite-ilmenite needles and platelets, and the similar crystal structure of hematite and ilmenite to corundum, suggest that the basal pinacoid direction of the inclusions and the host are parallel.

The edges of the magnetite plates had the same orientation as the hematite-ilmenite platelets. As shown in Figure 13, the magnetite plates commonly had triangular and hexagonal shapes. Since magnetite belongs to the spinel group, which crystallizes in the isometric crystal system, these shapes indicate a tetrahedral crystal habit.

Magnetite is known to be the most magnetic naturally occurring mineral. We tested the magnetism of the sapphires with neodymium-iron-boron magnets, and those containing large plates of magnetite were attracted to the magnets when the samples were floated in water (cf. Gumpesberger, 2006). A few low-quality sapphires possessing eye-visible magnetite inclusions were attracted to the magnets even without flotation (see Figure DD-8).

The Fe-Ti oxides and the diaspore-boehmite needles all formed in the sapphire as a result of epigenetic solid exsolution (cf. Hughes, 1997, pp. 93–94). Hematite, ilmenite and magnetite all have different chemical compositions, but they grew according to the crystallographic directions in the basal pinacoid of the host corundum. Such epigenetic inclusions crystallize due to the presence of defects and impurities of Fe and Ti in the host crystal as it cools after its formation (Hughes, 1997, pp. 93–94), forming microscopic needles and plate(let)s. The network of hematite-ilmenite inclusions in these sapphires is responsible for the asterism as well as the golden sheen.

As demonstrated above and verified through optical microscopy, the colour zoning in the sapphires is a consequence of the presence of hematite-ilmenite inclusions grouped into bands parallel to the second-order hexagonal prism {11$\bar{2}$0}. The resulting mechanical colour zoning is therefore linked to exsolution of these particles and also is epigenetic.

The dark-appearing veins following fractures in the Gold Sheen sapphires appear to have formed after the exsolution of Fe-Ti oxides. The exsolved inclusion particles evidently were not stable adjacent to (and on one side of) the fractures.

The presence of the long parallel white needles, identified as diaspore and boehmite, is correlated to the polysynthetic twin planes oriented in rhombohedral {10$\bar{1}$1} directions in the sapphire. In the literature, such inclusions are generally described as boehmite rather than diaspore (White, 1979; Hänni, 1987). Both diaspore and boehmite polymorphs of AlO(OH) were identified in our Raman spectra. They formed by the alteration of corundum at the intersections of two twin planes. Polysynthetic twin planes in corundum are created by mechanical stress after crystallization and are also known as slip twins (Hughes, 1997, p. 97). The angle of 58° between these twin planes and the basal pinacoid and 32° between the twin planes and the c-axis is consistent with the {10$\bar{1}$1} faces of the rhombohedral corundum.

Fe-Ti Oxide Inclusions in Other Gemstones

Plate-like inclusions of hematite and/or ilmenite also exist in other gem minerals. Their highly reflective surfaces produce optical effects such as aventurescence in oligoclase, often called *sunstone* (Gübelin and Koivula, 1986, pp. 165, 279; 2005, pp. 126, 413–415), and in cordierite (Gübelin and Koivula, 1986, pp. 163–164, 269; 2008, pp. 520–521). As in the Gold Sheen sapphires, the plate-like inclusions are parallel to the basal pinacoid. The cutting of the stones is such that the plates are oriented parallel to the girdle profile to highlight the optical effect. The abundance of the inclusions in the host also contributes to the body colour of the stones.

The aventurescence effect produces a kind of iridescence under oblique illumination, inducing various colours due to thin-film interference from the very thin plate-like inclusions. In oligoclase, beryl and cordierite, the inclusions are eye-visible, whereas in the Gold Sheen sapphires they are distinguishable

only with magnification. In the gems displaying aventurescence, the tiny reflective inclusions produce minute sparkles when the stone or the light source is moved. Gold Sheen sapphires display a golden shimmering effect originating from the specular reflections of light from the hematite-ilmenite inclusions. Instead of metallic single glitters, the microscopic network of oriented inclusions reflects light simultaneously, defining the golden sheen area. The smaller dimensions of the inclusions (below 100 µm) and their high concentration in the Gold Sheen sapphires account for the different appearances of the golden sheen and the aventurescence.

Comparison with Black Star Sapphires

Most cabochons of Gold Sheen sapphire display six-rayed asterism, similar to other star corundum. The presence of the asterism is dependent on the presence of oriented networks of hematite-ilmenite needles rather than platelets, and the sharpness of the star is determined by the aspect ratio of those needles. Since the hematite-ilmenite needles are perpendicular to the colour zoning, each ray of the star is, as a result, parallel to the colour zoning and to the second-order hexagonal prism $\{11\bar{2}0\}$. This optical characteristic is the same as that displayed by black star sapphires (Moon and Phillips, 1984; Hughes, 1997, p. 446). Those from Thailand, Australia and Laos are known to have inclusions caused by exsolution of hematite and ilmenite (Hughes, 1997, pp. 297, 380, 447).

In black 12-rayed star sapphires from Thailand, a less intense white six-rayed star is perpendicularly superimposed over a yellow/golden six-rayed star that originates from long, thin rutile needles aligned along the first-order hexagonal prism $\{10\bar{1}0\}$ (Hughes, 1997, p. 447). In our samples of Gold Sheen sapphire, no rutile needles perpendicular to the hematite-ilmenite needles were found by optical microscopy, and so far we have not encountered any 12-rayed stars in these cabochons.

Due to the high concentration of hematite-ilmenite inclusions in black star sapphires, some of these gems show basal parting on their flat base, characterized by a step-like appearance. Fractures due to this basal parting may be filled by residue from the dopping process during cutting (Hughes, 1997, pp. 125, 447). In Gold Sheen sapphires, no basal parting was seen in any of the cabochons. In a few faceted samples showing basal parting, the stones were completely opaque due to the high concentration of inclusions. As most Gold Sheen sapphires are translucent and not opaque, basal parting is not common.

Geological Inferences

Little information is available on the Gold Sheen sapphire deposit. According to the mine owner, it is located in eastern Kenya, near the border with Somalia. This area belongs to Kenya's North Eastern Province and has a low relief with an elevation less than 500 m. The climate is semi-arid, with desert scrub vegetation being most common. The geology of north-east and eastern Kenya is characterized by Mesozoic (Karoo) and Quaternary sedimentary rocks. The former includes Jurassic limestone, shale and gypsum, as well as Cretaceous siltstone, mudstone, limestone and sandstone. The Quaternary sediments are composed of lacustrine and fluvial deposits and gypsum. This entire region of East Africa is located on the Somali Plate, adjacent to the East African Rift and the Nubian Plate. Linear trends in the sedimentary rocks are orientated in relation to the Kenyan Dome (Mathu and Davies, 1996).

Kenya's previously known gem corundum deposits include the John Saul ruby mine located in Mangari (far south) and various other ruby and sapphire localities in the Mangari area, and the Turkana area in the north-western part of the country (Hughes, 1997, pp. 374–379; Shor and Weldon, 2009). To our knowledge, no corundum deposits have been reported in areas near Somalia.

The blue, green and yellow body colours of Gold Sheen sapphires are typical of magmatic-type corundum. Other magmatic deposits containing corundum with similar exsolved inclusions of Fe-Ti oxides are known from Australia (Anakie), Laos (Ban Huai Sai) and Thailand (Chanthaburi). The gemmological properties of black star sapphires from Australia and Thailand most closely resemble those of the Gold Sheen sapphire, including the high Fe content, lack of UV fluorescence, healed fractures and polysynthetic twinning. As there are no volcanic source rocks in the reported mining area for the Gold Sheen sapphires, their geological origin remains enigmatic.

Figure 15: Gold Sheen sapphires may create bold expressions in jewellery. The cabochon in this gold-plated silver pendant weighs 40–50 ct. Photo by T. K. Malik.

Conclusion

This article investigates the recently discovered Gold Sheen sapphires from East Africa, focusing on their peculiar golden sheen effect (e.g. Figure 15). Optical microscopy verified that the sheen is due to the reflection of light from an oriented network of exsolved needles and platelets of Fe-Ti oxides (hematite and ilmenite). The oriented needles also cause asterism (i.e. a six-rayed star) to be seen in cabochons cut from this sapphire.

Black star sapphires may contain similar oriented assemblages of exsolved Fe-Ti oxides. The main difference is the absence of rutile needles from the Gold Sheen sapphires, which explains the lack of 12-rayed asterism. Despite the presence of similar hematite-ilmenite inclusions in both types of sapphire, the large difference in their appearances suggests the need for further investigations into their optical phenomena.

An already-exhausted mine is the only known source of the Gold Sheen sapphires. Cutting of the existing stock of rough material is expected to fulfil market demand for the near future.

References

Bersani D. and Lottici P.P., 2010. Applications of Raman spectroscopy to gemology. *Analytical and Bioanalytical Chemistry*, **397**(7), 2631–2646, http://dx.doi.org/10.1007/s00216-010-3700-1.

de Faria D.L.A., Venâncio Silva S. and de Oliveira M.T., 1997. Raman microspectroscopy of some iron oxides and oxyhydroxides. *Journal of Raman Spectroscopy*, **28**(11), 873–878, http://dx.doi.org/10.1002/(sici)1097-4555(199711)28:11<873::aid-jrs177>3.3.co;2-2.

Guan X.-F., Zheng J., Zhao M.-L., Lia L.-P. and Li G.-S., 2013. Synthesis of $FeTiO_3$ nanosheets with {0001} facets exposed: Enhanced electrochemical performance and catalytic activity. *RSC Advances*, **3**(33), 13635–13641, http://dx.doi.org/10.1039/c3ra22125c.

Gübelin E.J. and Koivula J.I., 1986. *Photoatlas of Inclusions in Gemstones*. ABC Edition, Zurich, Switzerland, 532 pp.

Gübelin E.J. and Koivula J.I., 2005. *Photoatlas of Inclusions in Gemstones*, Vol. 2. Opinio Publishers, Basel, Switzerland, 829 pp.

Gübelin E.J. and Koivula J.I., 2008. *Photoatlas of Inclusions in Gemstones*, Vol. 3. Opinio Publishers, Basel, Switzerland, 672 pp.

Gumpesberger S.M., 2006. Magnetic separation of gemstones. *Gems & Gemology*, **42**(3), 124.

Hänni H.A., 1987. On corundums from Umba Valley, Tanzania. *Journal of Gemmology*, **20**(5), 278–284, http://dx.doi.org/10.15506/jog.1987.20.5.278.

Hughes R.W., 1997. *Ruby & Sapphire*. RWH Publishing, Boulder, Colorado, USA, 512 pp.

Kiefert L. and Karampelas S., 2011. Use of the Raman spectrometer in gemmological laboratories: Review. *Spectrochimica Acta Part A: Molecular and Biomolecular Spectroscopy*, **80**(1), 119–124, http://dx.doi.org/10.1016/j.saa.2011.03.004.

Laurs B.M., 2015. Gem Notes: 'Zawadi' sapphires. *Journal of Gemmology*, **34**(5), 393.

Mathu E.M. and Davies T.C., 1996. Geology and the environment of Kenya. *Journal of African Earth Sciences*, **23**(4), 511–539, http://dx.doi.org/10.1016/s0899-5362(97)00016-x.

Moon A.R. and Phillips M.R., 1984. An electron microscopy study of exsolved phases in natural black Australian sapphire. *Micron and Microscopica Acta*, **15**(3), 143–146, http://dx.doi.org/10.1016/0739-6260(84)90044-3.

Ruan H.D., Frost R.L. and Kloprogge J.T., 2001. Comparison of Raman spectra in characterizing gibbsite, bayerite, diaspore and boehmite. *Journal*

of Raman Spectroscopy, **32**(9), 745–750, http://dx.doi.org/10.1002/jrs.736.

Rull F., Martinez-Frias J., Sansano A., Medina J. and Edwards H.G.M., 2004. Comparative micro-Raman study of the Nakhla and Vaca Muerta meteorites. *Journal of Raman Spectroscopy*, **35**(6), 497–503, http://dx.doi.org/10.1002/jrs.1177.

Rull F., Martinez-Frias J. and Rodríguez-Losada J.A., 2007. Micro-Raman spectroscopic study of El Gasco pumice, western Spain. *Journal of Raman Spectroscopy*, **38**(2), 239–244, http://dx.doi.org/10.1002/jrs.1628.

Sharma Y.K., Kharkwal M., Uma S. and Nagarajan R., 2009. Synthesis and characterization of titanates of the formula $MTiO_3$ (M = Mn, Fe, Co, Ni and Cd) by co-precipitation of mixed metal oxalates. *Polyhedron*, **28**(3), 579–585, http://dx.doi.org/10.1016/j.poly.2008.11.056.

Shor R. and Weldon R., 2009. Ruby and sapphire production and distribution: A quarter century of change. *Gems & Gemology*, **45**(4), 236–259, http://dx.doi.org/10.5741/gems.45.4.236.

White J.S., 1979. Boehmite exsolution in corundum. *American Mineralogist*, **64**(11–12), 1300–1302.

Xu J.-A., Huang E., Lin J.-F. and Xu L.Y., 1995. Raman study at high pressure and the thermodynamic properties of corundum: Application of Kieffer's model. *American Mineralogist*, **80**(11–12), 1157–1165.

The Authors

Thanh Nhan Bui
Boulevard Edmond Machtens 180
1080 Brussels, Belgium
Email: tnhan93@gmail.com

Katerina Deliousi and Dr Katrien De Corte
HRD Antwerp, Institute of Gemmology
Hoveniersstraat 22, 2018 Antwerp, Belgium

Tanzim Khan Malik
Genuine Gems & Jewellery Co. Ltd.
316/9 Silom Road, Bangkok 10500, Thailand

Acknowledgements

The authors thank Dr Ellen Biermans and Ellen Barrie for EDXRF spectroscopy data. They are also grateful to Dr Ferran Ureña from the Catholic University of Louvain (Louvain-la-Neuve, Belgium) for the micro-Raman spectroscopy data. They express their sincere gratitude to Yiannis Karvelis for proofreading the English text.